This is a preprint, the final version is subject to change, of the American Mineralogist (MSA)
Cite as Authors (Year) Title. American Mineralogist, in press.
(DOI will not work until issue is live.) DOI: http://dx.doi.org/10.2138/am-2015-5181

Grain size measurement from two-dimensional micro-X-ray diffraction: Laboratory application of a radial integration technique

Michael S. Bramble[1*], Roberta L. Flemming[1], and Phil J. A. McCausland[1]

[1]Department of Earth Sciences, The University of Western Ontario, 1151 Richmond Street, London, Ontario, N6A 5B7, Canada. Correspondence e-mail: michaelbramble@gmail.com

This is a preprint, the final version is subject to change, of the American Mineralogist (MSA)
Cite as Authors (Year) Title. American Mineralogist, in press.
(DOI will not work until issue is live.) DOI: http://dx.doi.org/10.2138/am-2015-5181

Abstract

Two-dimensional X-ray diffraction data contain information about not only the type of mineral phases present in an assemblage, but also the textural or grain size relationships between minerals in a sample. For minerals within a certain grain size range, ~0.1 to 100 μm, the appearance and characteristics of a Debye ring can reveal the mean grain size of a sample. In this contribution, using mineral and rock samples of known grain size ranges, we investigate the applicability of calculating the grain size of a material using a two-dimensional X-ray diffraction crystallite size analysis method for micron-sized materials. A radial integration technique was used to derive the number of grains contributing to produce diffraction spots in the Debye ring. Monomineralic pyroxene and magnetite samples of known grain size ranges were analyzed, and the calculated grain size was observed to broadly correlate with the sample size except at the upper and lower extremes. To evaluate the technique on broader geological materials, polymineralic basalt samples with known grain size ranges were analyzed, and the calculated grain sizes did not correlate with the size of the rock fragments, but did correlate closely with the size of the individual mineral grains. Using a Bruker D8 Discover X-ray diffractometer with a 300 μm nominal incident beam diameter, the effectiveness of the applied method appeared limited to the grain size range of ~15–63 μm for monomineralic samples. The method is further limited by several complicating factors and assumptions, including the requirement for the crystallite size to correlate with the sample grain size. The effective range of this method will vary with different instrumental and experimental conditions. When applying this method to calculate the

grain size of geological materials, the calculated result should be interpreted as a minimum estimate of the grain size.

Keywords: micro-X-ray diffraction, two-dimensional X-ray diffraction, grain size, crystallite size, chi-profile, gamma-profile.

Introduction

Throughout the century-long history of X-ray diffraction, methods have been developed and applied to measure the size distribution of crystalline materials with two-dimensional X-ray diffraction (2D XRD) images by studying the characteristics of diffraction spots on the images and their relationship within a Debye ring. Deciphering the grain size relationships with the progression of smooth Debye rings to 'spotty' rings, and finally to large diffraction spots as the effective grain sizes of micron-sized minerals increased was pursued in two manners: (1) qualitative description of the Debye ring characteristics of minerals of known grain sizes with broad qualitative application to other minerals; and (2) more quantitative attempts to measure parameters from 2D XRD images and calculate a given grain size with some accuracy.

The qualitative method of grain size identification can be seen in the study of Debye-Scherrer X-ray diffraction film characteristics by several authors (e.g. Azároff and Buerger 1958; Klug and Alexander 1974; Cullity 1978) who presented observations of the visual qualities of the Debye rings of samples with known grain size to which samples with unknown grain size could then be compared. These observations can be

collectively summarized as follows: Below ~0.1 μm, Debye rings will display line broadening, and the lines will broaden with decreasing grain size until ~0.01 μm where the irradiated sample will begin a transition towards being X-ray amorphous. In the size range of 0.1 to 10 μm, a "perfect" powder X-ray diffraction pattern with thin, clearly discernible rings will exist, although there is not complete agreement on the exact transitions zones. Cullity (1978) stated that the transition from continuous rings without spots to spotty diffraction rings occurs between 1 μm and 10 μm, whereas Azároff and Buerger (1958) state that between 10 μm to 40 μm the sample has clearly discernable diffraction rings consisting of very many spots that are closely spaced. Klug and Alexander (1974) place continuous rings at <5 μm and spotty rings at 15 to 50 μm for quartz. Beyond ~50 μm Debye rings become progressively more discontinuous, and by ~200 μm or larger only a few diffraction spots are scattered on the film. Hörz and Quaide (1973) give a summary of Debye ring characteristics pertaining to the grain block size in several minerals.

In the finer grain size range where the Debye rings begin to broaden in the transition towards becoming X-ray amorphous, well-established quantitative methods of measuring the grain size of powdered materials exist (e.g. Klug and Alexander 1974; Rao and Houska 1986). These methods use data from one-dimensional diffractograms and derive the grain size from equations such as the Scherrer equation. With decreasing grain size, a nominally sharp diffractogram peak will begin to broaden at the base, and then broaden uniformly throughout (Azároff and Buerger 1958). With extensive broadening the peak height will decrease as well, and the area under the peak will remain constant (Azároff and Buerger 1958). Measuring these features and entering the results into the

Scherrer equation allows for the grain size to be inferred. The line profile method is particularly applicable when the grain size is below approximately 0.1 μm (He 2009).

Williamson and Hall (1953) combined equations for size and strain. The Rietveld whole pattern crystal structure refinement method (Rietveld 1969) also includes grain size and strain estimation (e.g. Balzar et al. 2004), and can refine on the crystal size of a sample in a method akin to the line profile method. Therefore, calculating grain size via the Rietveld method is applicable only for samples with grain size on the order of a few microns or smaller. Methods of crystallite size-lattice strain estimation from powder diffraction pattern line shapes were reviewed by Mittemeijer and Welzel (2008). One-dimensional powder diffraction methods were reviewed by Lavina et al. (2014). In the size range where the progression of changing Debye ring characteristics are seen, ~0.1 to 100 μm, the above methods are not applicable and other methods need to be applied.

Quantitative methods of deriving grain size from 2D XRD involve measuring parameters from 2D images and inputting these values into equations to calculate the grain size of the sample. Interestingly, in addition to their descriptions of Debye ring characteristics pertaining to grain size, Azároff and Buerger (1958) and Cullity (1978) both outline how a quantitative method for measuring grain size from these images could be attained. Their proposed methods were akin to the method applied in this study, but it likely took the advent of precise computer analysis of digital micro-X-ray diffraction (μXRD) images for the method to become a feasible reality.

Early quantitative methods of grain size measurement from 2D XRD are exemplified by Stephen and Barnes (1937). In applying a technique modified from Shdanow (1935), they measured the grain size of materials by the comparison of the

number of diffraction spots on two photographs taken with differing exposure times, or by counting the number of spots on one film taken under a standardized condition and comparing the result to an empirical chart. The calculation method was applied to six aluminum samples, and was shown to not be effective above 50 μm, but the region from 50 to 10 μm was shown to be useful, where results were found to agree within 10%. Hirsch and Kellar (1952) applied a more generalized version of the method developed by Stephen and Barnes (1937) for back-reflection patterns. Hirsch and Kellar (1952) stated that the method used in the study was more appropriate than the line profile method for materials which may have experienced strain, such as cold-rolled aluminum, because the textural information which coincides with the 2D XRD images allows for the calculated results to unequivocally be interpreted as grain size. The line profile method would require the assumption that the line broadening was solely the result of the grain size, a risky assumption when studying strained and deformed materials which can generate their own broadening features.

He (2009) formulated a modern method of calculating crystallite size from 2D XRD using multi-wire detectors and computer software, but also featuring many parallels with these earlier film-based techniques. Essentially, these methods calculate the volume of material irradiated by the X-ray beam using constraints such as the diameter of the X-ray beam and the X-ray absorption characteristics of the material, and divide this volume by the number of irradiated crystallites that were calculated in some manner to arrive at a calculated grain size. Here we present a laboratory investigation of the method of He (2009), applied with a micro-X-ray diffractometer with reflection-mode geometry, with the aims of exploring the applicability of this method in calculating the grain size of

This is a preprint, the final version is subject to change, of the American Mineralogist (MSA)
Cite as Authors (Year) Title. American Mineralogist, in press.
(DOI will not work until issue is live.) DOI: http://dx.doi.org/10.2138/am-2015-5181

geological materials in an X-ray diffraction laboratory, and constraining the degree to which differences in crystallite and grain size affect the method.

Methods and Materials

Grain size from 2D XRD after He (2009)

He (2009) formulated a method of crystallite size analysis that takes advantage of 2D XRD. This method, in its simplest form, relates the number of diffraction spots in a spotty diffraction ring and the sample volume to the size of the crystallites. On the image of the 2D XRD detector, a 2θ by χ angular window is selected for a particular Debye ring and is integrated along the χ direction. This produces an intensity versus χ plot which can then be fitted with a polynomial or line of the average intensity. Half the number of times the integrated profile crosses the plotted line is calculated as the number of crystallites diffracting in the window. When this number is related to the sample volume, the multiplicity of the diffracting plane, and the instrument parameters, the crystallite size can be calculated. This χ-profile analysis method is useful when applied to samples with crystallite sizes ranging from 0.1 μm to 100 μm, over the size range where Debye ring characteristics rapidly evolve with changing crystallite size. Note that He (2009) denominates this method as γ-profile analysis, but here we have used the term χ to correlate with the previous 2D XRD literature. The derivation of the crystallite size measurement that follows is taken from He (2009), and the reader is referred there for a thorough discussion.

This is a preprint, the final version is subject to change, of the American Mineralogist (MSA)
Cite as Authors (Year) Title. American Mineralogist, in press.
(DOI will not work until issue is live.) DOI: http://dx.doi.org/10.2138/am-2015-5181

The number of crystallites (N_s) contributing to a diffraction ring in a perfectly random powder can be given by

$$N_s = p_{hkl} \cdot \frac{V f_i}{v_i} \cdot \frac{\Omega}{4\pi} \qquad (1)$$

where the multiplicity of the diffraction ring is p_{hkl}, V is the effective sampling volume, f_i is the volume fraction of the crystallites being measured, v_i is the volume of the individual crystallites, and Ω is the instrument angular window. Including the multiplicity of the diffracting planes in the calculation allows for the mineral symmetry to be considered. When counting the number of crystallites contributing to a given diffraction ring, the multiplicity associated with the *hkl* index of the diffracting plane was taken into account, allowing for accurate accounting of the number of diffracting grains. The instrumental angular window can be expressed as

$$\Omega = \beta_1\beta_2 = 2\beta \arcsin[\cos\theta \sin(\Delta\chi/2)] \qquad (2)$$

where β_1 and β_2 are the instrument angular window in the 2θ and χ directions, respectively, and is related to the integration area on the 2D detector. The diffraction vector angular range corresponding to the azimuthal angular range can be expressed as $\Delta\chi$. β_1 can equal β for the window in the 2θ direction when instrumental broadening of the detector is neglected.

For the effective volume analyzed, several additional parameters need to be introduced. When data are collected with a coupled scan where θ_1 equals θ_2 (see below), the effective volume can be reduced to

$$V = \frac{A_0}{2\mu}, \qquad (3)$$

where μ is the linear absorption coefficient (see below).

This is a preprint, the final version is subject to change, of the American Mineralogist (MSA)
Cite as Authors (Year) Title. American Mineralogist, in press.
(DOI will not work until issue is live.) DOI: http://dx.doi.org/10.2138/am-2015-5181

Substituting Equations 2 and 3 into Equation 1, the crystallite volume of the *i*th phase can be expressed as

$$v_i = \frac{p_{hkl} f_i A_0 \beta \arcsin[\cos\theta \sin(\Delta\chi/2)]}{4\pi\mu N_s}. \quad (4)$$

Using the diameter of the crystallites (d),

$$v_i = \frac{\pi d_i^3}{6}, \quad (5)$$

to replace v_i, the crystallite size can then be expressed by

$$d = \left\{\frac{3 p_{hkl} f_i A_0 \beta \arcsin[\cos\theta \sin(\Delta\chi/2)]}{2\pi^2 \mu N_s}\right\}^{1/3}. \quad (6)$$

This formulation of the χ-profile crystallite size analysis was applied in this study. He (2009) also presents a version for transmission-mode geometry, as well as an alternate form of each employing a scaling factor that removes all of the numeric constants, simplifying the equation. This scaling factor can then be used as a calibration factor that can be set using 2D XRD data from a known standard.

The laboratory investigation herein explores the applicability of this method for measuring the grain size of a variety of geological samples typically analyzed in an X-ray diffraction laboratory. In this contribution, we apply the term grain size to identify the mean of the distribution of crystallite sizes in a geological sample, i.e. a powder, polished section, or hand sample. The use of the term grain size is somewhat varied in the geological sciences and can be used to describe many physical properties such as the size of individual mineral grains or crystals in coarse-grained igneous and metamorphic rocks as well as the size of rock particles consolidated into a fine-gained sedimentary rock. For the geological samples examined by μXRD in this study, we are applying a definition akin to the former, meaning that the mean size of mineral crystals in a sample will

This is a preprint, the final version is subject to change, of the American Mineralogist (MSA)
Cite as Authors (Year) Title. American Mineralogist, in press.
(DOI will not work until issue is live.) DOI: http://dx.doi.org/10.2138/am-2015-5181

approximately correlate with the mean grain size of a sample. However, in fine-grained rocks, the crystallite size, as measured by X-ray diffraction, will be smaller than the particle size of the rock. Thus, the application of this crystallite size calculation method should provide a minimum estimate of the grain size for all of these geological sample types, when this definition and other assumptions discussed below, are taken into consideration.

Micro-X-ray diffraction

The Bruker D8 Discover at the University of Western Ontario was used for this investigation, having theta-theta geometry, operating at 35 kV and 45 mA with a radiation source of Co*K*α (1.79026 Å), and a Göbel mirror with a 300 μm pinhole collimator. A HI-STAR detector with General Area Detector Diffraction System (GADDS; Bruker-AXS 2010) software was used. The sample-to-detector distance used was 12 cm. Applications of micro-X-ray diffraction (μXRD) in the geological sciences have shown it to be an effective technique for analyzing mineral textural information (Flemming 2007; Izawa et al. 2011; Bramble et al. 2014). The 2D frame windows were chosen so that the second frame was collected with the goniometer angles of both the source and the detector from the sample plane were both approximately 45°. A window in lower 2θ was also chosen to allow for comparison with the approximately 45° window, and because both magnetite and pyroxene have frequent and diagnostic XRD peaks in the range of 30 to 60 °2θ. The specific parameters used in this experiment employed a two frame coupled scan, where frame 1 was collected with $\theta_1 = \theta_2 = 20°$ and frame 2 was collected with $\theta_1 = \theta_2 = 29.5°$, and width = 19°. These parameters, when integrated,

generated an analysis range of 18–79 °2θ. The data collection time for each frame was 120 minutes. Unless specified otherwise, all data in this study were collected with the same instrumental parameters.

Omega scanning and sample oscillation

A key feature of μXRD is the versatility of the technique in the investigation of crystalline matter *in situ*, without sample preparation and with modifications as seen in the capabilities of omega scanning and sample oscillation. To constrain the effects of these method modifications on the grain size equation, a select set of the pyroxene and magnetite samples were analyzed by omega scan and sample oscillation in addition to the coupled scan method and the grain sizes were calculated for comparison. Testing these effects will aid in gauging the applicability of this grain size calculation method in situations where the sample or the optics are in motion during data collection (e.g. Blake et al. 2012).

Omega scanning is a feature of μXRD where the optics (source and detector) are simultaneously rotated in the same direction (clockwise) by a certain angle omega (ω) during data collection (see Flemming 2007). For each GADDS frame, the position of the source starts at a low θ_1 angle relative to the sample and is rotated by the goniometer to higher θ_1 angle relative to the sample (in degrees ω) while the detector, initially positioned at high θ_2 angle relative to the sample, is rotated to lower θ_2 (in degrees ω). The source and detector are rotated by the same omega angle at the same angular rate to maintain a constant 2θ position at the center of the detector (where $\theta_1 + \theta_2 = 2\theta$). Rotation of the optics enables more lattice planes to enter the correct geometry to satisfy Bragg's

law, mimicking the rotation of a sample under fixed source-detector optics. The objective of omega scanning is to increase the number of crystal lattices of a coarse-grained sample that are irradiated by the X-ray beam, producing diffracted rays that reach the detector. An omega scan will generate more diffracted spots on the detector for a particular mineral phase than an equivalent coupled scan.

The χ-profile grain size calculation was derived for a stationary optical geometry. This ensures that the window of area integrated on the detector directly matches the irradiated sample volume for a specific instrument geometry. An omega scan should increase the number of grains irradiated in a sample relative to the number measured in an equivalent coupled scan, and the N_s term should be similarly larger. This should result in the grain size calculation underestimating the grain size, because more grains will be counted and inserted into the equation than would be expected.

The micro-X-ray diffractometer used in this study also features a sample stage capable of moving up to 10 cm in X, Y, and Z directions. This sample stage allows for various materials to be placed on the stage and allows for spots of interest to be targeted and focused in three dimensions. This stage allows for samples to be oscillated in one, two, or three directions during data collection. Similar to the purpose of the omega scan, sample oscillation is intended to increase the number of different crystal lattices passing under the incident beam, which will then diffract X-rays towards the detector. Sample oscillation aims to generate data that would be akin to analyzing a powdered sample.

Similar to the expected effects of omega scanning, sample oscillation should increase the number of spots in a spotty ring for a given geometry than would be expected without sample oscillation. The result should be an increase in the N_s term for

the grain size calculation and subsequently an underestimation of grain size.

Materials

The pyroxene investigated in this study has the formula $[Mg_{1.753}Fe_{0.206}Ca_{0.025}Cr_{0.012}Mn_{0.004}Ni_{0.002}Co_{0.001}]_{\Sigma=2.003}(Si_{1.965}Al_{0.031})_{\Sigma=1.996}O_6$ and was a single large crystal that has been crushed and separated into 32 size fractions by dry and wet sieving for previous investigation of reflectance properties (e.g. Cloutis et al. 2008). The synthetic magnetite samples are from commercial sources and have been investigated in a previous study of magnetic property variation with grain size (Yu et al. 2002), which included a grain size analysis by scanning electron microscopy (SEM).

Columbia River Basalt sample SA-51, used in this study, was taken from a Roza Dike of Wallowa County, Oregon, of the United States of America. The Roza Member is a geological unit of the Columbia River Basalt Group (Martin 1989, 1991; Thordarson and Self 1998). This sample has been part of a geochemical analysis of the geological unit (Atkinson 1990) and has been studied with reflectance spectroscopy (Cloutis et al. 2008). The sample was also separated into 32 size fractions by dry and wet sieving. The χ-profile grain size analysis of this sample was performed to test the application of this method to multi-phase samples.

Data processing procedure

The analysis of the collected GADDS 2D images involved their integration to produce one-dimensional datasets. Initially, the entire frames were integrated normally to produce intensity versus 2θ plots. These were used to determine the exact location of

each Debye ring in 2θ space in order to index these from a relevant International Centre for Diffraction Data (ICDD) card, and determine the multiplicity of the diffracting plane.

Once the Debye rings and their multiplicities were identified, the frames were integrated along the Debye rings (χ dimension) to produce intensity versus χ plots. For consistency and comparison, the same Debye rings (i.e. diffraction vectors) were integrated for all samples of a given mineral. The integration windows were integrated by delineating a selected 2θ by χ angular window to include spotty rings (Fig. 1a); care was taken to avoid splitting any particularly large or bright spots. A few fractions of one degree of background 2θ area were integrated on each side of the ring so that all intensity across the full width of the ring was integrated.

The next step was to plot the χ-profiles along with a trend line (Fig. 1b). For the initial pyroxene dataset, both a second-degree polynomial and a linear average intensity line were used and the number of times the profile crossed the line (N_s) was counted for each. The polynomial often resulted in marginally higher numbers counted, but the linear trend produced more uniform results. Therefore, while this pyroxene application used both methods, the magnetite and basalt applications used only the average intensity line. The N_s term was calculated visually for the pyroxene dataset as well as using a threshold crossing algorithm to check the accuracy of the algorithm, which was then applied to the magnetite and basalt data. While this profile method may bias the N_s term towards grains above a certain size, it should remove contributions from complicating factors such as very fine mineral dust coating the samples, as was observed below in select pyroxene 2D XRD images.

The divergence angle of the collimator along the primary beam (β) was taken

from He (2009), where β for a 300 μm single pinhole collimator was given as 0.225 degrees. This value was entered into the grain size equation as 0.003927 radians. All calculations were performed with GNU Octave (Eaton et al. 2013).

The version of the χ-profile grain size measurement calculation applied in this study was the one derived for reflection geometry μXRD (He 2009). Therefore, the depth of X-ray penetration must be known to derive the volume irradiated. The calculation uses an area multiplied by height calculation where the area is the cross section of the beam and the depth is given by the linear absorption coefficient (μ) and the instrumental geometry. The linear absorption coefficients for all materials used in this study were calculated in GNU Octave, and the calculation used was taken from Ladd and Palmer (2003).

Rietveld refinement of basalt sample SA-51

To quantify the modal mineralogy of the SA-51 basalt sample, a Rietveld refinement was performed with data collected by a Rigaku Geigerflex D/MAX powder X-ray diffraction system. The interest of the refinement was to acquire approximate modal proportions of the major phases with an accuracy of a few weight percent. For analysis, a portion of the <10 μm sieve fraction of SA-51 was ground for one hour with an agate mortar and pestle to achieve a grain size less than approximately 5 μm. The ground sample was then placed in a sample holder with the aid of ethanol, which was allowed to dry. The Rigaku X-ray diffractometer was operated at 40 kV and 35 mA. Data were collected from 10–90 °2θ at a step size of 0.02 °2θ and a counting time of 42 s.

The Rietveld refinement was performed using the TOPAS software (version 3,

This is a preprint, the final version is subject to change, of the American Mineralogist (MSA)
Cite as Authors (Year) Title. American Mineralogist, in press.
(DOI will not work until issue is live.) DOI: http://dx.doi.org/10.2138/am-2015-5181

Bruker-AXS 2005). Phases were identified using the Bruker-AXS DIFFRACplus Evaluation software package in tandem with the Inorganic Crystal Structural Database (ICSD). Rietveld refinement is a non-linear least squares calculation that fits a calculated pattern to the observed diffraction data to determine crystal structural parameters for powdered materials (Rietveld 1967, 1969; Young 1993; Pecharsky and Zavalij 2005). The diffraction pattern peaks used the Thompson-Cox-Hastings pseudo-Voigt lineshape for modeling. We refined on zero error, sample displacement, and surface roughness, as well as scale and unit cell for each of the phases. Neither site occupancies nor the chemical compositions of the phases were altered from the original input structures.

In addition to crystal structure refinement, the method produces modal proportions of the phases in the refinement based on parameters such as the scaling factors and unit cell volume. While these abundances are highly dependent on the initial input parameters, they are accurate within a few percent, especially for fine-gained and homogenous materials.

Results

Application to well-characterized pyroxene

Table 1 displays the grain sizes calculated for the pyroxene samples analyzed using the polynomial (poly) and linear average intensity (lin) methods. A set of 2D images are shown in Figs. 2 and 3 that display the progression of Debye ring characteristics with increasing grain size, and images of the corresponding pyroxene samples are shown in Fig. 4. All grain size calculations for Debye rings from a particular

This is a preprint, the final version is subject to change, of the American Mineralogist (MSA)
Cite as Authors (Year) Title. American Mineralogist, in press.
(DOI will not work until issue is live.) DOI: http://dx.doi.org/10.2138/am-2015-5181

sieve size are also averaged into a single value for the size fraction for both the polynomial and average intensity values and are presented in their own column in Table 1, followed by their respective standard deviations. This process was followed for all of the data presented below.

The calculated grain sizes appear to broadly correlate with the sieve-size bins. It was difficult to draw conclusions about the "less than" sieve bins (e.g. <25 μm) because grain size did not have to fall within a specific limit. These sieves allowed for all material below the given limit to pass. The calculated sizes for the <25 and <20 μm samples do correlate with the sieve size, but the <10 and <5 μm samples are calculated above the sieve mesh size. The discrepancies may result from equation parameters (such as using a given beam divergence from He (2009)), or from the pyroxene physical properties that may have affected the sieving results, such as a stubby prismatic habit.

For many of the pyroxene sieve size bins with upper or lower limits, the calculated grain sizes correlate with the sieve size bins. The calculated grain sizes either fell within the sieve size bins or just outside the bin by ± ~5 μm. This was not true for the samples larger than 38 μm, where the calculated size tends to become significantly smaller than the bin size. These deviations in the larger sample sizes may be due to the above conditions, or may be a result of the instrumental setup. With the instrument geometry used in this study, the close detector distance may have caused the equation to significantly underestimate grain size (by ≥10 μm) as the sieve sizes increased above ~60 μm. This may be the result of fewer diffraction spots reaching the detector area for a given Debye ring. The standard deviations are similarly higher for the larger grain size samples and may reflect the uncertainty in measuring grain sizes above certain limits of

This is a preprint, the final version is subject to change, of the American Mineralogist (MSA)
Cite as Authors (Year) Title. American Mineralogist, in press.
(DOI will not work until issue is live.) DOI: http://dx.doi.org/10.2138/am-2015-5181

instrumental and physical conditions.

Table 1 shows the strong correlation between the polynomial and average intensity methods for the majority of the χ-profiles analyzed. For the samples below 38 μm, the difference in the calculated size between the polynomial and average intensity methods differs by 1 μm or less for the majority of the samples, and the sizes commonly overlap within the calculated standard deviations. As the sieve sizes grow above 38 μm the two methods begin to slightly diverge with the 38–45 and 75–90 μm dry sieve samples differing by about 5–6 μm between the polynomial and average intensity methods.

The visual analysis method of counting the number of times the χ-profile crossed the trend line proved to generate more consistent results for the average intensity method than the polynomial method. All of the following grain size calculations in this work use the average intensity method.

Application to well-characterized magnetite

The χ-profile grain size analysis was applied to a limited set of magnetite samples. The samples analyzed were of the following grain sizes: 0.065 ± 0.036 μm, 0.24 ± 0.07 μm, 1.06 ± 0.71 μm, and 18.2 ± 12.0 μm (see Fig. 5), which were measured by Yu et al. (2002) using SEM imaging. The χ-profile method was proposed to be applicable to grain sizes in the range of 0.1 to 100 μm (He 2009), but actual performance will vary within this range, depending on the instrumental parameters and sample properties. These samples will therefore be able to test the lower range of sizes calculable by this method.

The results of χ-profile analysis of these magnetite samples are shown in Table 2.

411 The measurement of the 18.2 ± 12.0 μm magnetite sample produced a result of 31.14 ±
412 7.43 μm, and other magnetite samples appear to suggest that the method does not
413 calculate accurate grain sizes when the samples are at or below 1 μm. He (2009)
414 suggested the applicability of the χ-profile method was in the range of 0.1 to 100 μm, but
415 the 0.065, 0.24, and 1.06 μm samples return approximately the same grain size of ~18
416 μm, suggesting that the problems arising with observation of the 0.065 and 0.24 μm
417 samples are also present with the 1.06 μm sample.

418 One possible explanation is that as the grain size decreases to 1 μm, and continues
419 with decreasing grain size to 0.065 μm and beyond, the spotty rings become more
420 continuous, and the number of grains providing spots in the detector window trends
421 asymptotically towards the pixel density of the detector. This is likely occurring in the
422 pyroxene samples as well, and may be why the grain size of the smaller samples appears
423 to level off at about 18 μm as the grain size continues to decrease (Table 1). If this
424 observation is correct, than the lower limit of applicability of the χ-profile method with
425 the instrumental geometry used in this study, and with the physical properties of the
426 magnetite samples, is perhaps closer to 18 μm rather than the proposed 0.1 μm (He
427 2009).

428 In the 2D image of the 0.065 μm sample, line broadening of the Debye rings is
429 observed. This visually occurs between the 0.24 μm and the 0.065 μm samples as shown
430 in Fig. 5. By analyzing the line broadening of these rings in 2θ, the grain size could be
431 calculated via the line profile method.

432 The larger calculated grain size for the pyroxene, with respect to sieve size bin for
433 the smaller sieve sizes, and the larger calculated grain size for magnetite, with respect to

This is a preprint, the final version is subject to change, of the American Mineralogist (MSA)
Cite as Authors (Year) Title. American Mineralogist, in press.
(DOI will not work until issue is live.) DOI: http://dx.doi.org/10.2138/am-2015-5181

SEM grain size for the smaller grain sizes, both appear to result from erroneous circumstances with the equations. As the pyroxene sieve sizes became smaller, the calculated grain sizes began to level off at about 15 μm. No pyroxene grain size was calculated below ~14 μm. It is possible that the window that is integrated in χ becomes saturated as the grains are approaching ~15 μm, and as the grains pass below this size (~15 μm) the N_s term trends asymptotically towards that of a smooth Debye ring. The magnetite grains suggest that this hypothesis is correct, because for the 18.2 μm magnetite sample, the observed grain size correlates with the calculated grain size within given uncertainties, but for the three smaller samples (1.06 μm and below), approximately the same grain size was calculated (~18 μm). In this case we are simply measuring the χ-profile of a smooth ring, which would not contain any grain size information in the χ-dimension.

Omega scanning and sample oscillation

A test of the effects of the omega scan method (rotating optics) was executed on four samples. Three binned pyroxene samples of sieve sizes 10–15, 20–25, and 25–38 μm, and one magnetite sample (18.2 ± 12.0 μm) were analyzed. A two-frame omega scan was employed, with $\theta_1 = 15°$, $\theta_2 = 25°$, and $\omega = 10°$ for the first frame, and $\theta_1 = 19°$, $\theta_2 = 40°$, and $\omega = 25°$ for the second frame. To produce similar quality data as were collected for the stationary pyroxene and magnetite above, the data were collected for 120 min per frame.

The results of the χ-profile grain size calculations of the omega-scanned samples are shown in Table 3 along with the corresponding grain sizes for the coupled-scanned

This is a preprint, the final version is subject to change, of the American Mineralogist (MSA)
Cite as Authors (Year) Title. American Mineralogist, in press.
(DOI will not work until issue is live.) DOI: http://dx.doi.org/10.2138/am-2015-5181

(stationary) samples. The sizes measured from the omega scan correlate strongly with the sizes measured from the coupled scan, but they all underestimate the coupled scan sizes as the above theory suggested. The omega scan of the 10–15 μm pyroxene sample falls within the sieve size bin, but the two larger-sized samples have their omega scan sizes fall about 5 μm below the lower limit of the bin size. The omega scan magnetite sample was calculated to be about 6 μm below the coupled scan (stationary) sample, but the omega scan size is actually closer to the size measured by SEM (though both calculated sizes fall within the uncertainty of the magnetite SEM size).

The effects of sample oscillation were investigated by analyzing the four samples analyzed using the omega scan above. The coupled scan method was applied, and the samples were oscillated in the Y direction by 3.5 mm during data collection.

The results of the χ-profile grain size calculations on the oscillated samples are shown in Table 4 along with the corresponding grain sizes for the non-oscillated samples. The observations of the oscillated data were similar to those of the omega scan data. As the theory suggested, the data collected while oscillating underestimated the calculated grain size as compared to that calculated for same samples when not oscillated. This was true for all pyroxene samples analyzed as they underestimated their non-oscillated sizes by up to ~5 μm. The magnetite sample was also underestimated by ~7 μm, but, as was seen with the omega scan data for magnetite, the oscillated sample was closer to the magnetite grain size as measured by SEM.

Application to the Roza Member—Columbia River Basalt Group

Using the same parameters for data collection as the pyroxene and magnetite,

Roza Member basalt samples that were sieved into size fractions with an upper and lower limit were analyzed with the Bruker D8 Discover μXRD diffractometer. The 2D XRD frames were analyzed in the same manner as the data presented above.

As the basalt samples are composed of multiple mineral phases, the χ-profile grain size equation required an estimate of the modal fraction of the selected mineral in the assemblage. The modal proportion is entered into the equation as the *fi* term, which is the modal fraction of the *i*th mineral phase.

The results of the Rietveld refinement for modal mineralogy and the initial structures employed are given in Table 5. The R_{wp} value of the calculation was 10.6. This refinement was executed only to ascertain the approximate modal proportions of the major phases present. For a thorough crystal structure refinement, a refinement with stronger fit statistics and smaller step size would be required. Only the two most abundant basalt phases, anorthite (60 %) and augite (23 %), were used for the grain size calculation.

Multiple phases in the collected diffraction pattern displayed preferred orientation, the evidence of which was observed to continue into the residual from the refined pattern. The preferred orientation was likely a result of sample preparation. Grinding the sample for one hour may have not created a homogeneous assortment of crystallites, especially for the anorthite and augite which likely remained somewhat lath-like. Preferred orientation was expected as the crushed basalt sample was suspended in ethanol in the sample holder, which was then allowed to dry. As the interest in the refinement was to acquire approximate modal proportions of the major phases with an accuracy of a few weight percent, preferred orientation was not taken into consideration

nor refined in this calculation.

The calculated grain sizes for a set of sieved SA-51 basalt samples are shown in Table 6. In contrast to our previous applications of the χ-profile method, the majority of the SA-51 grain sizes for anorthite and augite calculated did not correlate with the sieve size bins. The smaller sieve sizes up to the 15–20 μm sieve size did correlate with the calculated grain sizes, within their standard deviations. The overall characteristic of the χ-profile grain sizes appears that they seem to converge at a value of about 13–14 μm, even in the 63–75 μm sieve size fraction of the sample. This was especially apparent when a 'whole rock' grain size was calculated by averaging all the calculated grain sizes for different minerals in a single sieve size sample. One standard deviation of this 'whole rock' grain size for all sieve sizes analyzed is 1.41 μm.

Roza Member basalt samples appear to be composed of agglomerated minerals of ~13–14 μm in size that dominate the calculated grain size, regardless of the rock particle size (sieve size), whether the minerals occur as separate grains or as part of a larger rock. This is expected, as X-rays will only investigate the size of coherent scattering domains of the mineral grains or crystallites within the rock fragment and not size of the larger rock fragments. The mineral grain size of the rock fragments was measured qualitatively by reflected light petrography and appeared to agree with the ~14 μm grain size calculated by the χ-profile method.

Difficulty arose in integrating particular Debye rings for these samples as it was not straightforward which particular spots belonged to which mineral phase. This occurred, in part, because basalt consists of multiple minerals with low symmetry. The low symmetry causes the mineral to have a low multiplicity that results in the mineral

This is a preprint, the final version is subject to change, of the American Mineralogist (MSA)
Cite as Authors (Year) Title. American Mineralogist, in press.
(DOI will not work until issue is live.) DOI: http://dx.doi.org/10.2138/am-2015-5181

having many closely-spaced Debye rings (cf. Figs. 2 and 3 with Fig. 5). A mixture of minerals of relatively low symmetry made it difficult to avoid overlapping diffraction spots. Additionally, augite and pigeonite have many diffraction peaks at similar 2θ locations. The augite Debye rings used for the basalt grain size calculations were at 40.7 and 41.5 °2θ, which were also the approximate locations of similar intensity pigeonite peaks. Some proportion of the augite diffraction spots used to calculate grain size in this study may in fact have been due to pigeonite peaks, and therefore the uncertainty in these calculations is increased.

Further difficulty arose from the size of spots on the 2D images of multi-phase materials. Frequently, the XRD spots were so large in area that they spanned an entire degree of 2θ, making the identity of particular diffraction spots difficult for multi-phase materials. This was particularly difficult for the larger sieve size fractions, where the Debye rings were discontinuous and individual diffraction spots were large.

Discussion

Progression of Debye ring characteristics with decreasing grain sizes

Our collected data on the suite of pyroxene samples allows us to observe the changing characteristics of Debye rings with changes in grain size (see Figs. 2 and 3). For the 38–45 μm seive sample and larger grain size samples, large diffraction spots are observed on the image and distinct Debye rings are not discernible. In accordance with Azároff and Buerger's (1958) observation for samples 80 μm and larger in grain size, we

see that the diffraction spots may be deviating somewhat from the Debye ring diffraction vectors. With the additional difficulty of the low symmetry of pyroxene, it can be difficult to index large diffraction spots in data for pyroxene grains that are 38 μm or larger in size.

Beginning at approximately 38 μm sieve fraction, the shape of the Debye rings becomes more discernible with decreasing grain size. The diffraction spots continue to have significant spacing between them, and this continues with decreasing grain size to about the 20 μm sieve fraction. Beginning at about 20 μm, the Debye rings become more continuous, but retain a spotty, often discontinuous appearance. A low intensity, somewhat-continuous ring was seen with very high intensity smaller diffraction spots embedded in the ring. Depending on the intensity of these high intensity spots, the lower intensity spots may not be significant enough to count as a grain in the χ-profile analysis.

The <5 μm sample, which was twice ground for one hour in this study, displays the most continuous rings of all the pyroxene samples. Note that these rings are still highly discontinuous and at times highly spotty. The <5 μm sample continues to display sporadic diffraction spots of relatively high intensity embedded in the rings. This is likely the result of a distribution of grain sizes contained in each sieved sample.

Selected results from our findings here are in contrast to selected literature observations of spotty Debye rings. In the introduction, several qualitative observations relating Debye ring characteristics to grain size were presented. For example, Cullity (1978) stated that for grain sizes from 10 to 1 μm there was a transition from spotty diffraction rings to continuous rings without spots. Similarly, Hörz and Quaide (1973)

stated that samples in the range of 0.2 to 10 μm should display "smooth rings, perfect powder pattern". While we did observe this behaviour in the two magnetite samples that bracket this range, it was not observed in the pyroxene samples. Our <5 μm pyroxene data cannot be described as continuous rings without spots, nor as a perfect powder pattern.

Hörz and Quaide (1973) also stated that their samples in the range of 10 to 40 μm displayed "clearly discernible diffraction lines". This Debye ring behaviour was not clearly observed in our pyroxene data. In the range of 10 to 40 μm discernible rings begin to appear but they remain strongly discontinuous.

These differing observations of Debye ring characteristics on 2D XRD images as a function of grain size suggest that the qualitative method of constraining the grain size of a sample by comparison of ring characteristics with literature observations should be done with caution. A potential source of the discrepancies between our observations and the literature may be the result of the difference between a Debye-Scherrer film camera and a HI-STAR multi-wire detector. Our detector has a diameter of 11.5 cm and a resolution up to 1024 pixels along this diameter. A film camera has a width of ~2.5 cm. Other sources of variance between the Debye-Scherrer observations and those of this study may be the use of different sample preparation methods, or the difference in X-ray beam diameters applied in each system, which would result in different irradiated sample volumes. As a result of the scaling involved between the different sample-to-detector distances, the beam diameters employed, and imaging areas involved in the two methods, it is possible that some of our discontinuous Debye rings would become smoother in film cameras, and result in our discrepancies from the film-based grain size literature.

This is a preprint, the final version is subject to change, of the American Mineralogist (MSA)
Cite as Authors (Year) Title. American Mineralogist, in press.
(DOI will not work until issue is live.) DOI: http://dx.doi.org/10.2138/am-2015-5181

Similarly, the degree to which the grain size of a sample correlates with its crystallite size will also affect the relationship of Debye ring characteristics as a function of grain size. If the sample is not well constrained in this manner and the correlation is not strong then there could be great variability at which grain size changes in the progression of ring characteristics occurs.

Complications of sample heterogeneity

Samples that display a variation in grain size or mineralogy complicate the χ-profile grain size analysis method; the primary reason being that the method analyzes only a small volume of sample. A sample can fill a large sample holder but the method will only analyze a volume equal to the area of the beam times either the depth of penetration or the thickness of the transmission sample holder.

Voluminous or varied samples create a circumstance where the volume irradiated may not be representative of the sample. For example, if the sieve size is 20–25 μm with an uncertainty of about 10 μm above or below the size bin, the small irradiated volume may give a grain size of 10 μm or 35 μm, neither of which might be representative of the whole. To limit the error due to sample inhomogeneity, we recommend collecting data at multiple locations on larger samples, and averaging the grain size over these irradiated volumes to provide a more representative calculated grain size. Analyzing data collected at multiple targets of a single sample for comparison was employed in the magnetite sample analysis in this study.

Variation in sample composition can also affect the certainty of the grain sizes

615 calculated due to the presence of the linear absorption coefficient in the calculation of
616 irradiated sample volume. Composition variation was shown to have a minor effect when
617 the variation was small. For example, when cation substitutions are on the order of a few
618 tens of percent the variation in calculated grain size can be on the order of a few microns.
619 This was confirmed by replacing the end-member enstatite ($MgSiO_3$) composition by a
620 pyroxene with the composition measured by microprobe (see Materials section above) in
621 the calculation. Little change was seen between the two calculated datasets. The change
622 in crystal chemistry resulted in a decrease in the calculated grain sizes of about one
623 micron or less for many of the samples, with the exception of few where the pyroxene
624 composition caused a drop of a few microns. The addition of iron into the equation
625 caused the linear absorption coefficient to marginally drop, corresponding to the X-ray
626 beam irradiating a smaller volume of material. Therefore, when the calculation was
627 executed assuming the same number of crystallites contributing to the Debye ring, the
628 calculated grain size was smaller.

629 For samples with larger chemical variation, or uncertain chemical nature, the
630 volume of material analyzed may be greatly affected by the absorption characteristics of
631 all the materials in the irradiated volume. If the linear absorption coefficient used in the
632 calculation does not reflect the absorption characteristics of the minerals analyzed, the
633 calculated volume irradiated, and the corresponding grain size, will be incorrect.

634

635 **Complications of multi-phase materials**

636 The χ-profile grain size analysis method becomes more complicated when applied

This is a preprint, the final version is subject to change, of the American Mineralogist (MSA)
Cite as Authors (Year) Title. American Mineralogist, in press.
(DOI will not work until issue is live.) DOI: http://dx.doi.org/10.2138/am-2015-5181

637 to multi-phase materials with multiple minerals and varying modal mineralogies. With
638 single-phase materials, the method assumes that the diffraction spots correspond to the
639 entire irradiated volume divided into a corresponding number of grains per spots with
640 factors taken into consideration such as multiplicity. Multi-phase materials will subdivide
641 the calculated irradiated volume further to represent the volume fraction of the phase of
642 interest in the sample. This can be done by including the modal proportion of the mineral
643 in the grain size calculation.

644 Several concerns and complications arise from the inclusion of modal mineralogy.
645 To acquire modal mineralogy of a sample, time intensive and perhaps expensive
646 techniques are needed. A common method is Rietveld refinement, but for certain rock
647 types other methods such as normative mineralogy could be used. Rietveld refinement
648 requires high quality data that are not easily acquired using the Bruker D8 Discover
649 (Ning and Flemming 2005), and may require grinding the sample to provide the small
650 grain sizes needed for Rietveld-quality data as well as analyzing the sample on another
651 instrument. Both situations were used for the basalt sample analyzed in this study.

652 For mixtures in reflection-mode geometry, the effectiveness of measuring the
653 irradiated volume by incorporating the linear absorption coefficient must be questioned.
654 The separate phases in a sample will each have distinct absorption characteristics, and,
655 depending on the variations in atoms, the individual minerals may have greatly differing
656 linear absorption coefficients. The χ-profile method assumes that, when measuring the
657 grain size of a particular mineral using its modal mineralogy, only the linear absorption
658 of this particular mineral must be employed. This is questionable for the X-rays will be
659 interacting with, and altered by, the absorption characteristics of all of the phases

encountered, especially if the sample is not completely homogenous. The situation is more complex than the χ-profile method assumes. It changes the effective volume to suit a particular circumstance of absorption and modal mineralogy when measuring one particular mineral, and then allows the volume and absorption to change again when measuring a different Debye ring for a different mineral in the same 2D image.

Multi-phase materials pose a significant homogeneity problem for samples of larger grain sizes for the mixture of minerals being analyzed by the beam may not necessarily correlate with a modal mineralogy measured on a finely ground sample. When the grain size approaches ~50 μm, the microscope context camera on the Bruker D8 Discover shows that only the upper minerals will be targeted by the beam (see Fig. 4g and 4h). The small size of the beam (nominally 300 μm) suggests that the small volume of material analyzed will not correlate with the bulk modal mineralogy, and thus the calculated grain sizes will be inaccurate. As the grain size of the material analyzed approaches a significant proportion of the X-ray beam footprint, the heterogeneity of multi-phase materials may induce significant errors in the grain sizes calculated.

Similarly, He (2009) states that smaller X-ray beam cross sections should be employed for accurate measurements. For the above reasons, multi-phase materials will induce errors with smaller beam footprints for they will potentially subsample fewer phases. An optimal crossover point may exist between the accuracy derived by smaller cross sections and the need to sample a representative portion of multi-phase materials. Further investigation of multi-phase materials is needed to constrain the above effects.

We reiterate that the χ-profile method cannot be used to calculate the particle size

This is a preprint, the final version is subject to change, of the American Mineralogist (MSA)
Cite as Authors (Year) Title. American Mineralogist, in press.
(DOI will not work until issue is live.) DOI: http://dx.doi.org/10.2138/am-2015-5181

682 of rock fragments, because the diffracted X-rays relate to the individual irradiated
683 mineral grains in a sample. The surface of a rock particle will be composed of multiple
684 lattice planes corresponding to the constituent mineral grains. The X-rays will be
685 diffracted by these various planes and generate a 2D image that reflects the sum of
686 individual mineral grains in the rock sample, and not the particle size of the bulk sample.
687 As a rock is ground more finely, eventually the mineral grain size is reached (~13 μm in
688 the case of Columbia River basalt), and the calculated grain size will correspond to the
689 particle size of the heterogeneous material analyzed (i.e. the sieve size). As the rock is
690 ground even finer, the particle size and crystallite size will decrease simultaneously, and
691 the calculated grain size by XRD will correlate with the sieve size, as was moderately
692 observed in the basalt dataset. More study is needed to aid in refining the application of
693 this method to multi-phase materials.
694
695 **Grain versus crystallite size assumptions**
696 For the above application of the χ-profile technique, we used the collected data
697 from this crystallite size analysis technique to make inferences about the grain size of the
698 samples. This assumption that the grain size of a sample and the coherent scattering
699 domain size are the same may be the greatest limitation of applying this method to
700 geological materials. In some cases, these two physical properties may coincide, but the
701 provenance of and preparation techniques applied to many geological materials may
702 exacerbate the disagreement between the coherent scattering domains of a mineral and
703 the grain size calculated.
704 The correlation between the coherent scattering domains and observable grain

and subgrains via other analytical measurement techniques, such as transmission electron microscopy, suggests that there may not be a direct correlation between these phenomena (e.g. Ungár et al. 2005). The presence of subgrains or small coherent scattering domains within a mineral grain may bias a grain size measurement towards reporting sizes that are smaller than the seemingly apparent whole grain. From this perspective, our observations may be influenced by the subgrains present in the mineral samples. When applying this method to calculate the grain size of the many types of geological materials, if taken from a range where the method is known to be effective, the calculated result should be interpreted as a minimum estimate of the grain size.

Certain observations could be made to constrain the strength of the assumption that the grain size and coherent X-ray scattering domains correlate via 2D XRD images. For example, a crystal, when experiencing strain or shock processes, will undergo a transition from a discrete spot on a 2D XRD detector to a spot that will streak out until a point where the strained lattice resolves into a series of discrete subgrains (Flemming 2007; Vinet et al. 2011; Izawa et al. 2011). The end result of clustered subgrains displays an asterism pattern on the 2D XRD image (Flemming 2007; Vinet et al. 2011). Therefore, it is possible to infer some degree of subgrain formation via 2D XRD data. We have not observed spatially clustered diffraction spots akin to asterism in the data presented herein, supporting that the mineral grains have not been exceedingly disrupted into small subgrains. The crushing and sieving of the pyroxene samples could reasonably induce defects into the crystals leading to poor correlation between the sieve size and the actual grain size of the individual particles in the powders. The magnetite samples were characterized by SEM, but despite the more-quantitative SEM characterization of

magnetite than sieving of pyroxene, the calculated grain sizes of each agreed with the observed grain size at approximately the same correlation level.

Implications

Effective range of χ-profile grain size analysis

He (2009) states that the χ-profile crystallite size calculation method should be effective for materials in the range of 0.1–100 μm. The findings from our investigation suggest that, when applied to calculate the grain size of varied geological materials, this range should be constrained in both its upper and lower limit for reflection-mode geometry μXRD.

The upper limit should be lowered to about 63 μm, especially for closer sample-to-detector distance as was used in this study. We found that the technique began to significantly under-report grain sizes for samples larger than 63 μm. The 45–63 μm pyroxene sample was the largest sample to provide grain size calculation that correlated with sieve size. The grain size calculated for this sample was 56.77 ± 24.68 μm. The 75–90 μm sample, for example, gave a calculated grain size of 42.12 ± 22.63 μm. This may be the result of not having enough grains diffracting at orientations within the limited circumference of the Debye ring on the area detector to provide a statistically significant χ-profile thus not providing a representative number of diffraction spots. The measurement of only the partial Debye rings that fall within the 2D detector is a potentially limiting factor of this method.

The lower limit results from saturating the detector, as discussed briefly above. As the pyroxene and magnetite grain sizes grew smaller, the calculated grain size appeared to trend asymptotically toward a value of about 15 μm. Therefore, as grain sizes approach this value, which may vary depending on the material being analyzed, caution should be employed. Certain instrumental conditions, such as a larger sample-to-detector distance or different beam footprint, may allow for smaller grain sizes to be calculated, but in the instrumental setup used in this study, the lower limit appears to have been about 15 μm. Further experiments in measuring grain sizes in the range of 0.1 to 15 μm would greatly benefit the efficacy of the χ-profile grain size measuring method.

In the grain size range of 15–63 μm, the χ-profile method of measuring grain size via reflection geometry μXRD appears to be moderately successful at providing an estimate of the sample grain sizes. The reflection-mode version of this equation does appear to be hindered by the many inherent free parameters and numerical constants required for the calculation and the physics and geometry involved with multi-phase materials. The method can provide a minimum estimate of the calculated grain size that is accurate within several microns of the mean grain size under specific instrumental conditions, but the requirement of modal mineralogy for multi-phase materials may limit the effectiveness of this technique.

In calculating the grain size of geological materials, this method may be limited to measuring monomineralic materials and further limited by heterogeneities of bulk samples. The scope of this method may be limited to highly characterized and uniform samples where the variation in constituent grains is small. The scope may be further limited in its laboratory application of grain size measurement due to the assumption that

773 the coherent scattering domains correlate with the overall grain size of the sample, due to
774 instrumental factors that may be influencing the results, and likely other factors requiring
775 further investigation. If a particular sample were heavily influenced by subgrain
776 formation, then the grain sizes measured by the above method would correlate with the
777 coherent scattering domains of the crystallites and not closely related to the grain size of
778 the sample as measured by geological methods such as sieving.

779 In the geological and planetary sciences, 2D XRD has been increasing in use as a
780 method of quantifying the strain and shock levels of materials via the progression of 2D
781 XRD characteristics of minerals as they are shocked or strained by impacts or other
782 planetary processes. To further advance these and other analyses, understanding the grain
783 size of the samples being analyzed is of great importance, and being able to analyze the
784 grain size of a sample *in situ* via 2D μXRD will be valuable. Similarly, the study of
785 planetary materials will benefit from the further development of a method of constraining
786 the grain size of a sample via non-destructive and sample-preparation-free methods, such
787 as μXRD.

788

789 **Acknowledgments**

790

791 This manuscript was much improved by the insightful comments of Jim Britten
792 and an anonymous reviewer. Michael Craig and Ed Cloutis are thanked for providing the
793 sieved pyroxene and SA-51 Roza Member basalt samples. David Dunlop and Ozden
794 Özdemir are thanked for providing the synthetic magnetite size fraction samples used in
795 this study. We also thank Matthew Izawa, Michael Craig, and Jeff Berger for the

countless insightful discussions. This work utilized a publicly available threshold-crossing algorithm written by Steffen Brueckner. Funding to RLF and PJAM from the Natural Sciences and Engineering Research Council of Canada (NSERC) is acknowledged.

References

Atkinson, S. S. (1990). Geochemical and Isotopic Study of the Roza Member Feeder System, Columbia River Basalt Group. M.Sc. thesis, University of Alberta, Edmonton, AB, Canada.

Azároff, L. V., and Buerger, M. J. (1958). The powder method in X-ray crystallography, 342 p. New York: McGraw-Hill.

Balazar, D., Audebrand, N., Daymond, M. R., Fitch, A. Hewat, A., Langford, J. I., Le Bail, A Louër, D., Masson, O., McCowan, C. N., Popa, N. C., Stephens, P. W., and Toby, B. H. (2004). Size-strain line-broadening analysis of the ceria round-robin sample. Journal of Applied Crystallography. 37, 911–924.

Blake, D., Vaniman, D., Achilles, C., Anderson, R., Bish, D., Bristow, T., Chen, C., Chipera, S., Crisp, J., Des Marais, D., Downs, R. T., Farmer, J., Feldman, S., Fonda, M., Gailhanou, M., Ma, H., Ming, D. W., Morris, R. V., Sarrazin, P., Stolper, E., Treiman, A., and Yen, A. (2012). Characterization and Calibration of the CheMin Mineralogical Instrument on Mars Science Laboratory. Space Science Reviews, 170, 341–399.

818 Blake, R. L., RE, H., Zoltai, T., and Finger, L. W. (1966). Refinement of hematite
819 structure. American Mineralogist, 51, 123.
820 Bosi, F., Hålenius, U., and Skogby, H. (2009). Crystal chemistry of the magnetite-
821 ulvöspinel series. American Mineralogist, 94, 181–189.
822 Bramble, M. S., Flemming, R. L., Hutter, J. L., Battler, M. M., Osinski, G. R., and
823 Banerjee, N. R. (2014). A temperature-controlled sample stage for in situ micro-
824 X-ray diffraction: Application to Mars analog mirabilite-bearing perennial cold
825 spring precipitate mineralogy. American Mineralogist 99, 943-947.
826 Bruker-AXS. (2005). TOPAS V3: General profile and structure analysis software for
827 powder diffraction data. Bruker-AXS, Karlsruhe, Germany.
828 Bruker-AXS. (2010). DIFFRACplus Evaluation Package Release 2010. Bruker-AXS,
829 Karlsruhe, Germany.
830 Camara, F., Carpenter, M. A., Domeneghetti, M. C., and Tazzoli, V. (2003). Coupling
831 between non-convergent ordering and transition temperature in the C2/c ↔ P21/c
832 phase transition in pigeonite. American Mineralogist, 88, 1115–1128.
833 Clark, J. R., Appleman, D. E., and Papike, J. J. (1969). Crystal-chemical characterization
834 of clinopyroxenes based on eight new structure refinements. Mineralogical
835 Society of America Special Paper 2, 31–50.
836 Cloutis, E. A., McCormack, K. A., Bell III, J. F., Hendrix, A. R., Bailey, D. T., Craig, M.
837 A., Mertzman, S. A., Robinson, M. S., and Riner, M. A. (2008). Ultraviolet
838 spectral reflectance properties of common planetary minerals. Icarus, 197, 321–
839 347.

840 Cullity, B. D. (1978). Elements of X-ray diffraction, 2nd ed. p. 555. Reading, MA:
841 Addison-Wesley Pub. Co.
842 Eaton, J. W., Bateman, D., and Hauberg, S. (2013). GNU Octave version 3.8.0 manual: A
843 high-level interactive language for numerical computations.
844 Facchinelli, A., Bruno, E., and Chiari, G. (1979). The structure of bytownite quenched
845 from 1723 K. Acta Crystallographica Section B Structural Crystallography and
846 Crystal Chemistry, 35, 34–42.
847 Fjellvåg, H., Grønvold, F., Stølen, S., and Hauback, B. (1996). On the Crystallographic
848 and Magnetic Structures of Nearly Stoichiometric Iron Monoxide. Journal of
849 Solid State Chemistry, 124, 52–57.
850 Fleet, M. E., and Pan, Y. (1997). Site preference of rare earth elements in fluorapatite;
851 binary (LREE+HREE)-substituted crystals. American Mineralogist, 82, 870–877.
852 Flemming, R. L. (2007). Micro X-ray diffraction (μXRD): a versatile technique for
853 characterization of Earth and planetary materials. Canadian Journal of Earth
854 Sciences, 44, 1333–1346.
855 He, B. B. (2009). Two-dimensional X-ray diffraction, 426 p. Hoboken, N.J: Wiley.
856 Hirsch, P. B., and Kellar, J. N. (1952). A study of cold-worked aluminium by an X-ray
857 microbeam technique. I. Measurement of particle volume and misorientations.
858 Acta Crystallographica, 5, 162–167.
859 Hörz, F., and Quaide, W. L. (1973). Debye-scherrer investigations of experimentally
860 shocked silicates. The Moon, 6, 45–82.

Izawa, M. R. M., Flemming, R. L., Banerjee, N. R., and McCausland, P. J. A. (2011). Micro-X-ray diffraction assessment of shock stage in enstatite chondrites. Meteoritics and Planetary Science, 46, 638–651.

Klug, H. P., and Alexander, L. E. (1974). X-ray diffraction procedures for polycrystalline and amorphous materials, 2d ed. p. 966. New York: Wiley.

Ladd, M. F. C., and Palmer, R. A. (2003). Structure determination by X-ray crystallography, 4th ed., p. 819. New York: Kluwer Academic/Plenum Publishers.

Lavina, B., Dera, P. and Downs, R.T. (2014). Modern X-ray diffraction methods in mineralogy and geosciences. Reviews in Mineralogy and Geochemistry, **78**, 1-31.

Martin, B. S. (1989). The Roza Member, Columbia River Basalt Group; Chemical stratigraphy and flow distribution. Geological Society of America Special Papers, 239, 85–104.

Martin, B. S. (1991). Geochemical variations within the Roza Member, Wanapum Basalt, Columbia River Basalt Group: Implications for the magmatic processes affecting continental flood basalts, 531 p. PhD thesis, University of Massachusetts - Amherst, U.S.A.

Merli, M., Oberti, R., Caucia, F., and Ungaretti, L. (2001). Determination of site population in olivine: Warnings on X-ray data treatment and refinement. American Mineralogist, 86, 55–65.

Mittemeijer, E.J., and Welzel, U. (2008). The “state of the art” of the diffraction analysis of crystallite size and lattice strain. Zeitschrift für Kristallographie, 223, 552-560.

Ning, G., and Flemming, R.L. (2005). Rietveld refinement of LaB6: Data from μXRD. Journal of Applied Crystallography, 38, 757-759.

884 Pecharsky, V. K., and Zavalij, P. Y. (2005). Fundamentals of powder diffraction and
885 structural characterization of materials, 713 p. Boston; London: Kluwer Academic
886 Publishers.
887 Rao, S., and Houska, C. R. (1986). X-ray particle-size broadening. Acta
888 Crystallographica Section A, 42, 6–13.
889 Rietveld, H. M. (1967). Line profiles of neutron powder-diffraction peaks for structure
890 refinement. Acta Crystallographica, 22, 151–152.
891 Rietveld, H. M. (1969). A profile refinement method for nuclear and magnetic structures.
892 Journal of Applied Crystallography, 2, 65–71.
893 Rossi, G., Smith, D. C., Ungaretti, L., and Domeneghetti, M. C. (1983). Crystal-
894 chemistry and cation ordering in the system diopside-jadeite: A detailed study by
895 crystal structure refinement. Contributions to Mineralogy and Petrology, 83, 247–
896 258.
897 Schdanow, H. S. (1935). Bestimmung der Kornzahl im Bereiche von 1 bis 100 μ auf
898 Grund der Debye–Scherrer–Aufnahmen. Zeitschrift für Kristallographie, 90, 82–
899 91.
900 Stephen, R. A., and Barnes, R. J. (1937). The estimation of grain-size in the region above
901 10-3 cm. Journal of the Institute of Metals, 60, 285–301.
902 Sueno, S., Cameron, M., and Prewitt, C. T. (1976). Orthoferrosilite; high-temperature
903 crystal chemistry. American Mineralogist, 61, 38–53.
904 Thordarson, T., and Self, S. (1998). The Roza Member, Columbia River Basalt Group: A
905 gigantic pahoehoe lava flow field formed by endogenous processes? Journal of
906 Geophysical Research: Solid Earth, 103, 27411–27445.

907 Young, R.A. (1993). Editor. The Rietveld Method, 298 p. Oxford; New York: Oxford
908 University Press.
909 Yu, Y., Dunlop, D. J., and Özdemir, Ö. (2002). Partial anhysteretic remanent
910 magnetization in magnetite 1. Additivity. Journal of Geophysical Research: Solid
911 Earth, 107, EPM 7–1–EPM 7–9.
912 Vinet, N., Flemming, R. L., and Higgins, M. D. (2011). Crystal structure, mosaicity, and
913 strain analysis of Hawaiian olivines using in situ X-ray diffraction. American
914 Mineralogist, 96, 486–497.
915 Ungár, T., Tichy, G., Gubicza, J., and Hellmig, R. J. (2005). Correlation between
916 subgrains and coherently scattering domains. Powder diffraction, 20, 366–375.
917 Williamson, G.K. and Hall, W.H. (1953). X-ray line broadening from filed aluminium
918 and wolfram. Acta Metallurgica. 1, 22–31.
919
920
921
922
923
924
925
926
927
928
929

This is a preprint, the final version is subject to change, of the American Mineralogist (MSA)
Cite as Authors (Year) Title. American Mineralogist, in press.
(DOI will not work until issue is live.) DOI: http://dx.doi.org/10.2138/am-2015-5181

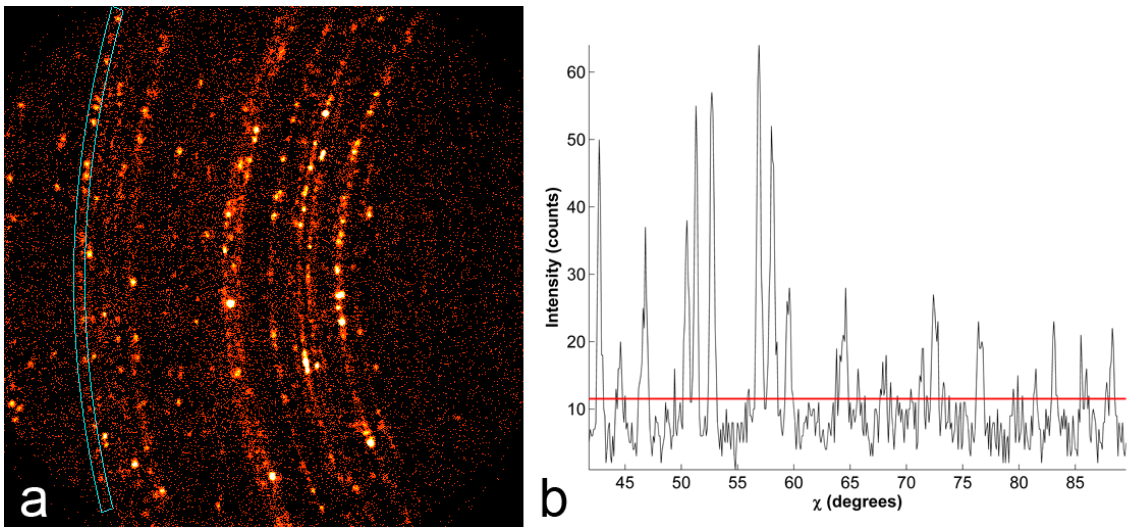

Figure 1: A two-dimensional X-ray diffraction frame (a) with a selected window to be integrated in χ. The frame is of a 10–15 μm wet sieve size pyroxene. The corresponding χ-profile is shown (b) in a plot of intensity versus χ. An average intensity line is plotted (red) and every two times the χ-profile intersects this average intensity line is counted as a single grain.

This is a preprint, the final version is subject to change, of the American Mineralogist (MSA)
Cite as Authors (Year) Title. American Mineralogist, in press.
(DOI will not work until issue is live.) DOI: http://dx.doi.org/10.2138/am-2015-5181

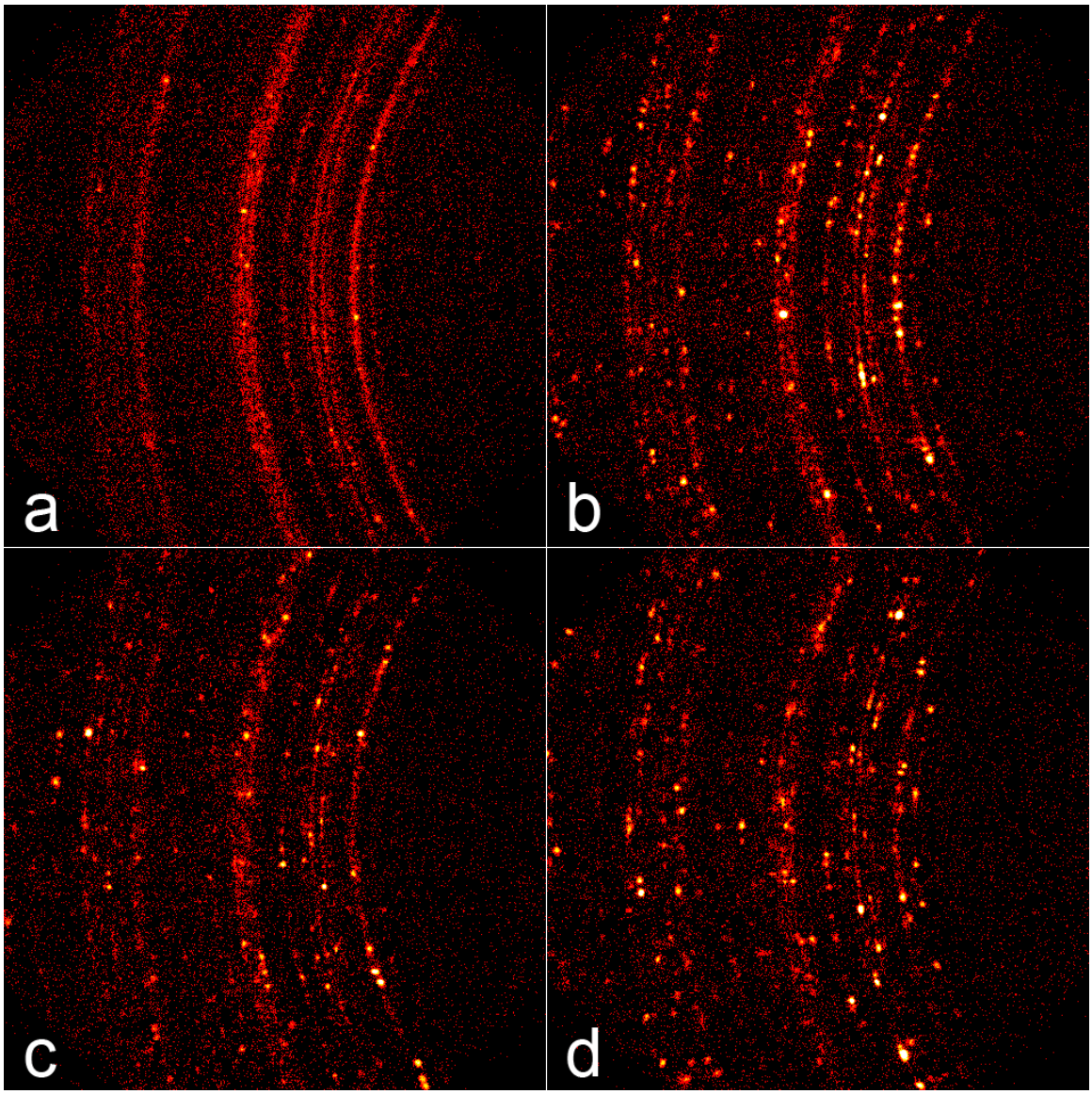

Figure 2: Two-dimensional X-ray diffraction images of pyroxene samples of increasing sieve size. Frames are shown for pyroxenes of wet sieve sizes (a) <5, (b) 10–15, (c) 15–20, and (d) 20–25 μm.

This is a preprint, the final version is subject to change, of the American Mineralogist (MSA)
Cite as Authors (Year) Title. American Mineralogist, in press.
(DOI will not work until issue is live.) DOI: http://dx.doi.org/10.2138/am-2015-5181

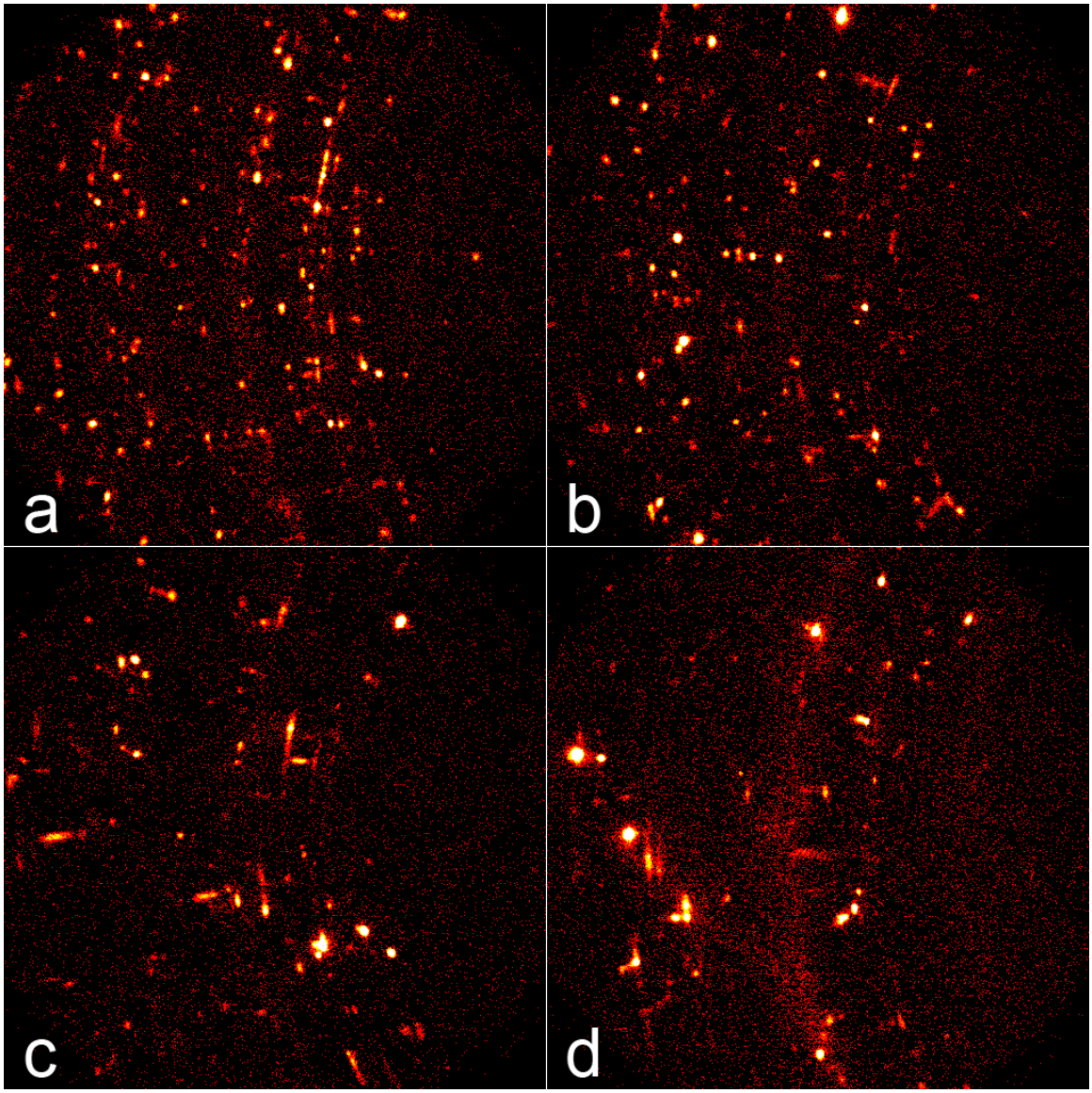

Figure 3: Two-dimensional X-ray diffraction images of pyroxene samples of increasing sieve size. Frames are shown for pyroxenes of dry sieve sizes (a) 25–38, (b) 38–45, (c) 45–63 μm, and (d) 90–125 μm. Note: Broad, diffuse Debye rings seen in the images are likely due to fine-grained dust-sized particles of pyroxene generated during the original crushing of the sample, as the sample was not washed after crushing.

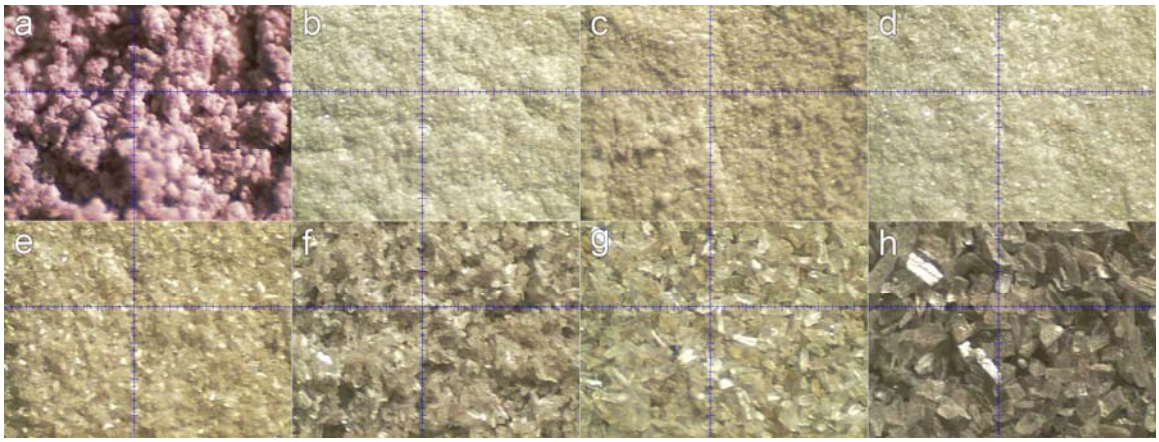

Figure 4: Context microscope camera images showing targeted locations for micro-X-ray diffraction. Images shown are pyroxene samples of increasing grain size. A sample passing the <10 μm wet sieve was ground twice for one hour to an assumed size of approximately (a) <5 μm is shown under different lighting conditions than the remaining images. Frames are shown for pyroxenes of wet sieve sizes (b) 10–15 μm, (c) 15–20 μm, and (d) 20–25 μm, and dry sieve sizes (e) 25–38 μm, (f) 38–45 μm, (g) 45–63 μm, and (h) 90-125 μm. Minor ticks on the crosshairs denote 50 μm. These images correspond to the two-dimensional X-ray diffraction images in Figs. 2 and 3.

This is a preprint, the final version is subject to change, of the American Mineralogist (MSA)
Cite as Authors (Year) Title. American Mineralogist, in press.
(DOI will not work until issue is live.) DOI: http://dx.doi.org/10.2138/am-2015-5181

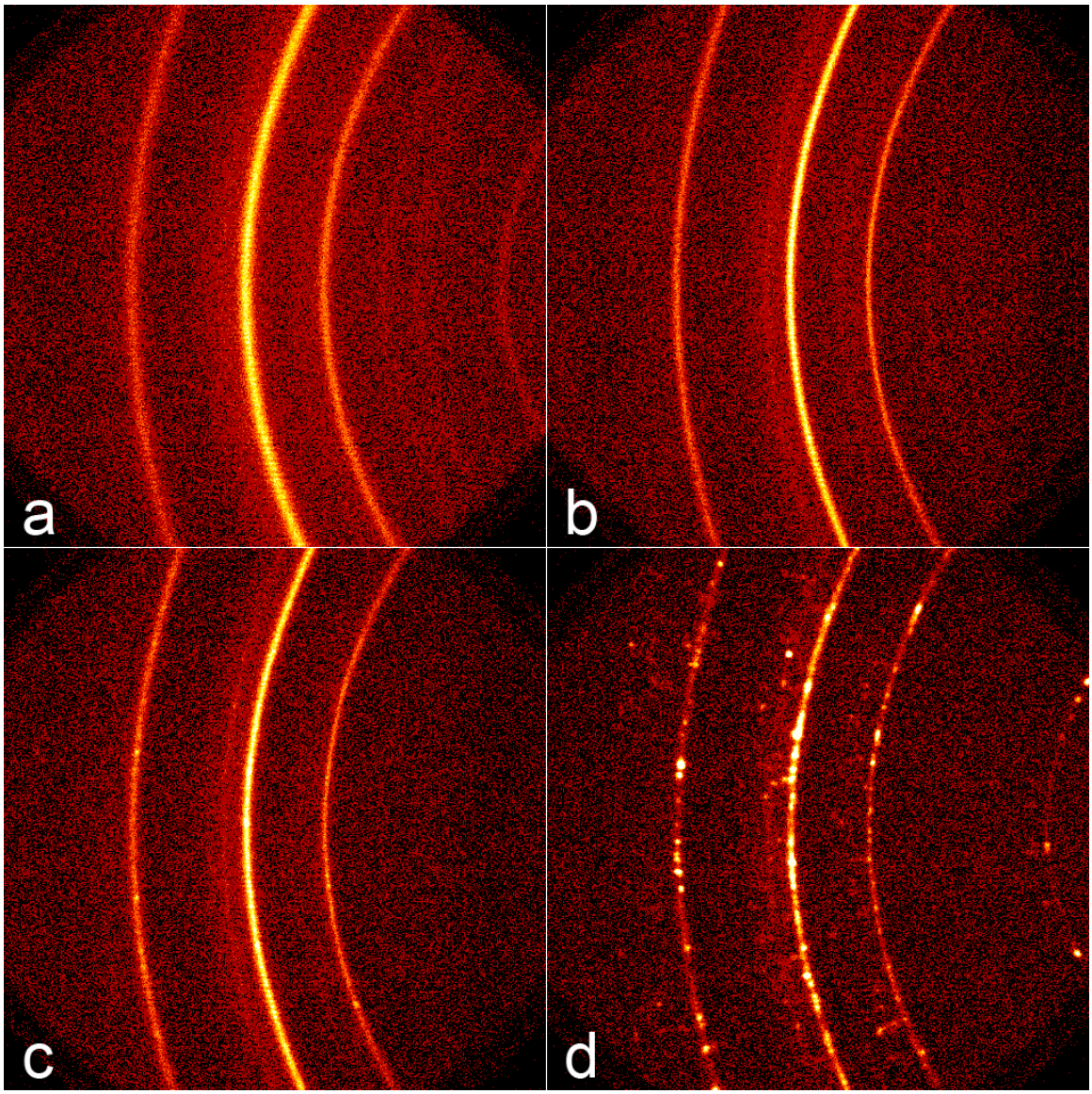

Figure 5: Two-dimensional X-ray diffraction images of magnetite samples of increasing size. Frames are shown for samples of grain size (a) 0.065 ± 0.036, (b) 0.24 ± 0.07, (c) 1.06 ± 0.71, and (d) 18.2 ± 12.0 μm, as measured by scanning electron microscopy by Yu et al. (2002).

977 Table 1: Grain sizes of sieved pyroxene samples as calculated by χ-profile grain size
978 analysis.

Sieve size (μm)	Avg. calc. poly (μm)	SD (μm)	Avg. calc. lin. (μm)	SD (μm)
<5 wet, ground	**15.76**	1.34	**15.79**	1.24
<10 wet	**17.97**	1.32	**18.44**	2.60
<20 dry	**17.77**	0.38	**17.34**	0.99
<25 dry	**22.73**	2.52	**24.35**	3.91
10 - 15 wet	**20.22**	2.14	**20.85**	2.57
15 - 20 wet	**18.56**	3.70	**19.26**	4.99
20 - 25 wet	**22.32**	0.48	**23.15**	1.40
25 - 38 wet	**21.63**	7.05	**22.35**	6.27
25 - 38 dry	**25.88**	4.24	**28.27**	5.77
38 - 45 dry	**22.70**	6.07	**28.01**	10.68
75 - 90 dry	**36.16**	20.67	**42.12**	22.63

979

980 Notes: Samples are identified by the sieve size used and whether they were wet or dry
981 sieved. A value averaging the grain size from multiple Debye rings for the sample is
982 given as well as the standard deviation (SD). This process was executed for both the
983 polynomial dataset ('poly') and the linear average intensity line dataset ("lin.").

984

985 Table 2: Magnetite grain sizes as measured by scanning electron microscopy (SEM; Yu
986 et al. 2002) and calculated by χ-profile grain size analysis.

SEM size (μm)	Calc. (μm)	SD (μm)
0.065 ± 0.036	18.36	4.28
0.24 ± 0.07	18.53	4.37
1.06 ± 0.71	19.58	4.66
18.2 ± 12.0	31.14	7.43

987

988 Note: The sample averaged calculated size (Calc.) is given along with the standard
989 deviation (SD).

990 Table 3: Grain sizes of non-omega-scanned and omega scanned pyroxene and magnetite
991 samples. The samples are identified by either their wet sieve size (in μm) for pyroxene, or
992 scanning electron microscopy size for magnetite. The χ-profile calculated grain sizes are
993 given along with the standard deviations (SD).

Original	**Calc. (μm)**	**SD (μm)**
10-15	20.85	2.57
20-25	23.15	1.40
25-38	22.35	6.27
18.2 ± 12.0	31.14	7.43
Omega scan	**Calc. (μm)**	**SD (μm)**
10-15	16.77	0.63
20-25	17.56	1.07
25-38	19.44	2.04
18.2 ± 12.0	24.79	5.64

994

995

996 Table 4: Grain sizes of non-oscillated and oscillated pyroxene and magnetite samples.
997 The samples are identified by either their wet sieve size (in μm) for pyroxene, or
998 scanning electron microscopy size for magnetite (also in μm). The χ-profile calculated
999 grain sizes are given along with the standard deviations (SD).

Original	**Calc. (μm)**	**SD (μm)**
10-15	20.85	2.57
20-25	23.15	1.4
25-38	22.35	6.27
18.2 ± 12.0	31.14	7.43
Oscillated	**Calc. (μm)**	**SD (μm)**
10-15	16.86	0.87
20-25	18.67	1.06
25-38	21.74	1.49
18.2 ± 12.0	24.57	5.34

1000

1001

Table 5: The results of the Rietveld refinement for modal mineralogy of the SA-51 basalt sample. The mineral phases employed in the refinement, their initial structure references, and the weight percent proportions are given.

Phase	Reference	wt.%
Anorthite	Facchinelli et al. 1979	60
Augite	Clark et al. 1969	23
Apatite	Fleet and Pan 1997	3
Magnetite	Fjellvag et al. 1996	3
Olivine	Merli et al. 2001	3
Pigeonite	Camara et al. 2003	3
Hematite	Blake et al. 1966	2
Orthopyroxene	Sueno et al. 1976	2
Ulvospinel	Bosi et al. 2009	1

Table 6: Grain sizes of sieved basalt samples as calculated by χ-profile grain size analysis. Samples are identified by their sieve size, and whether they were wet or dry sieved. For each sieve size, the calculated grain size for each mineral is given, as well as an averaged value for the entire sample ("Whole rock"). Uncertainties are given as calculated by the standard deviation (SD). The N/A denotes a grain size consisting of a single Debye ring measurement.

Sieve Size (μm)	Anorthite (μm)	SD (μm)	Augite (μm)	SD (μm)	Whole rock (μm)	SD (μm)
less than 10	13.09	N/A	10.45	1.01	11.11	1.56
10 to 15 wet	16.34	9.98	11.91	2.03	13.69	5.73
15 to 20 wet	21.52	N/A	11.55	0.41	14.04	5.00
20 to 25 wet	9.88	1.57	15.97	6.33	12.93	5.30
25 to 38 wet	13.59	9.57	13.33	5.82	13.46	7.09
38 to 45 dry	9.51	2.43	12.60	6.13	11.06	4.50
45 to 63 dry	15.67	10.93	14.45	8.58	14.94	8.19
63 to 75 dry	14.52	8.85	13.80	9.09	14.09	7.81